RESEARCH ARTICLE

QUANTUM GASES

Observation of many-body localization of interacting fermions in a quasirandom optical lattice

Michael Schreiber,[1,2] Sean S. Hodgman,[1,2] Pranjal Bordia,[1,2] Henrik P. Lüschen,[1,2] Mark H. Fischer,[3] Ronen Vosk,[3] Ehud Altman,[3] Ulrich Schneider,[1,2,4] Immanuel Bloch[1,2]*

Many-body localization (MBL), the disorder-induced localization of interacting particles, signals a breakdown of conventional thermodynamics because MBL systems do not thermalize and show nonergodic time evolution. We experimentally observed this nonergodic evolution for interacting fermions in a one-dimensional quasirandom optical lattice and identified the MBL transition through the relaxation dynamics of an initially prepared charge density wave. For sufficiently weak disorder, the time evolution appears ergodic and thermalizing, erasing all initial ordering, whereas above a critical disorder strength, a substantial portion of the initial ordering persists. The critical disorder value shows a distinctive dependence on the interaction strength, which is in agreement with numerical simulations. Our experiment paves the way to further detailed studies of MBL, such as in noncorrelated disorder or higher dimensions.

The ergodic hypothesis is one of the central principles of statistical physics. In ergodic time evolution of a quantum many-body system, local degrees of freedom become fully entangled with the rest of the system, leading to an effectively classical hydrodynamic evolution of the remaining slow observables (*1*). Hence, ergodicity is responsible for the demise of observable quantum correlations in the dynamics of large many-body systems and forms the basis for the emergence of local thermodynamic equilibrium in isolated quantum systems (*2*–*4*). It is therefore of fundamental interest to investigate how ergodicity breaks down and to understand the long-time stationary states that ensue in the absence of ergodicity.

One path to breaking ergodicity is provided by the study of integrable models, in which thermalization is prevented owing to the constraints imposed on the dynamics by an infinite set of conservation rules. Such models have been realized and studied in a number of experiments with ultracold atomic gases (*5*–*7*). However, integrable models represent very special and fine-tuned situations, making it difficult to extract general underlying principles.

Theoretical studies over the past decade point to many-body localization (MBL) in a disordered isolated quantum system as a more generic alternative to thermalization dynamics. In his original paper on single-particle localization, Anderson already speculated that interacting many-body systems subject to sufficiently strong disorder would also fail to thermalize (*8*). Only recently, however, have convincing theoretical arguments been put forward that Anderson localization remains stable under the addition of moderate interactions, even in highly excited many-body states (*9*–*11*). Further theoretical studies have established the many-body localized state as a distinct dynamical phase of matter that exhibits previously unknown universal behavior (*12*–*22*). In particular, the relaxation of local observables does not follow the conventional paradigm of thermalization and is expected to show explicit breaking of ergodicity (*23*).

Although Anderson localization of noninteracting particles has been experimentally observed in a variety of systems, including light scattering from semiconductor powders in three-dimensional (3D) (*24*), photonic lattices in 1D (*25*) and 2D (*26*), and cold atoms in 1D and 3D random (*27*–*29*) and quasirandom (*30*) disorder, the interacting case has proven more elusive. Initial experiments with interacting systems have focused on the superfluid- (*31*–*33*) or metal-to-insulator (*34*) transition in the ground state. Evidence for inhibited macroscopic mass transport was reported even at elevated temperatures (*34*) but is hard to distinguish from the exponentially slow motion expected from conventional activated transport or effects stemming from the inhomogeneity of the cloud. Possible precursors of MBL have also been reported in a transport experiment by using conventional thin-film electronic insulators (*35*).

Here, we report the experimental observation of ergodicity breaking because of MBL away from the ground state. Our experiments are performed in a 1D system of ultracold fermions in a bichromatic, quasirandomly disordered lattice potential. We identified the many-body localized phase by monitoring the time evolution of local observables following a quench of system parameters. Specifically, we prepared a high-energy initial state with a strong, artificially prepared charge density wave (CDW) order (Fig. 1A) and measured the relaxation of this CDW in the ensuing unitary evolution. Our main observable is the imbalance $\mathcal{I}$ between the respective atom numbers on even (N_e) and odd (N_o) sites

$$\mathcal{I} = \frac{N_e - N_o}{N_e + N_o} \quad (1)$$

which directly measures the CDW order. Although the initial CDW ($\mathcal{I} \sim 0.9$) will quickly relax to zero in the thermalizing case, this is not true in a localized system, in which ergodicity is broken and the system cannot act as its own heat bath (Fig. 1B) (*36*). Intuitively, if the system is strongly localized, all particles will stay close to their original positions during time evolution, thus only smearing out the CDW a little. A longer localization length ξ corresponds to more extended states and will lead to a lower steady-state value of the imbalance. The long-time stationary value of the imbalance thus effectively serves as an order parameter of the MBL phase and allows us to map the phase boundary between the ergodic and nonergodic phases in the parameter space of interaction versus disorder strength. In particular, close to the transition, the imbalance is expected to vanish asymptotically as a power law $\propto 1/\xi^{\alpha}$ with $\alpha > 0$ (*37*). In contrast to previous experiments, which studied the effect of disorder on the global expansion and transport dynamics (*27*, *30*, *31*, *33*, *34*), the CDW order parameter acts as a purely local probe, directly capturing the ergodicity breaking. Although ultimately facing a similar challenge, namely distinguishing very slow dynamics from no dynamics, the CDW is expected to undergo much faster dynamics, facilitating the detection of MBL.

Theoretical model

Our system can be described by the 1D fermionic Aubry-André model (*38*) with interactions (*36*), given by the Hamiltonian

$$\hat{H} = -J\sum_{i,\sigma}(\hat{c}^{\dagger}_{i,\sigma}\hat{c}_{i+1,\sigma} + \text{h.c.}) + \Delta\sum_{i,\sigma}\cos(2\pi\beta i + \phi)\hat{c}^{\dagger}_{i,\sigma}\hat{c}_{i,\sigma} + U\sum_{i}\hat{n}_{i,\uparrow}\hat{n}_{i,\downarrow} \quad (2)$$

Here, J is the tunneling matrix element between neighboring lattice sites, $\hat{c}^{\dagger}_{i,\sigma}$ denotes the creation operator, and $\hat{c}_{i,\sigma}$ denotes the annihilation operator for a fermion in spin state $\sigma \in \{\uparrow, \downarrow\}$ on site i. The second term describes the quasirandom disorder—the shift of the on-site energy due to an additional incommensurate lattice, characterized

[1]Fakultät für Physik, Ludwig-Maximilians-Universität München, Schellingstrasse 4, 80799 Munich, Germany. [2]Max-Planck-Institut für Quantenoptik, Hans-Kopfermann-Strasse 1, 85748 Garching, Germany. [3]Department of Condensed Matter Physics, Weizmann Institute of Science, Rehovot 7610001, Israel. [4]Cavendish Laboratory, University of Cambridge, J. J. Thomson Avenue, Cambridge CB3 0HE, UK.
*Corresponding author. E-mail: imb@mpq.mpg.de

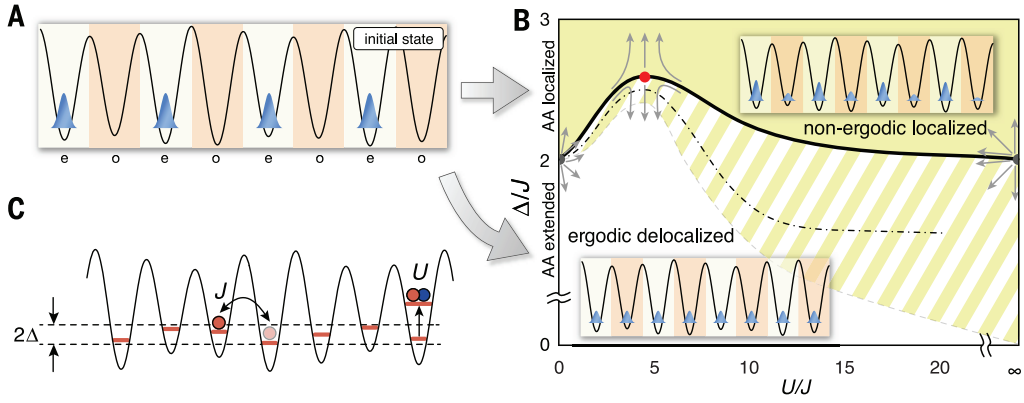

Fig. 1. Schematics of the many-body system, initial state, and phase diagram. (**A**) Initial state of our system consisting of a CDW, in which all atoms occupy even sites (e) only. For an interacting many-body system, the evolution of this state over time depends on whether the system is ergodic or not. (**B**) Schematic phase diagram for the system. In the ergodic, delocalized phase (white), the initial CDW quickly decays, whereas it persists for long times in the nonergodic, localized phase (yellow). The striped area indicates the dependence of the transition on the doublon fraction, with the black solid line indicating the case of no doublons. The black dash-dotted line represents the experimentally observed transition for a finite doublon fraction, extracted from the data in Fig. 4. The gray arrows depict the postulated pattern of renormalization group flows controlling the localization transition. For $U = 0$, as well as in the limit of infinite U with no doublons present (*37*), the transition is controlled by the noninteracting Aubry-André critical point, represented by the unstable gray fixed points. Generically, however, it is governed by the MBL critical point (*48*), shown in red. The $U = 0$ and $U = \infty$ as well as the $\Delta/J = 0$ limits represent special integrable cases that are not ergodic (*51*, *52*). (**C**) A schematic representation of the three terms in the Aubry-André Hamiltonian (Eq. 2).

by the ratio of lattice periodicities β, disorder strength Δ, and phase offset ϕ. Finally, U represents the on-site interaction energy, and $\hat{n}_{i,\sigma} = \hat{c}^{\dagger}_{i,\sigma}\hat{c}_{i,\sigma}$ is the local number operator (Fig. 1C).

This quasirandom model is special in that for almost all irrational β (*37*), all single-particle states become localized at the same critical disorder strength $\Delta/J = 2$ (*38*). For larger disorder strengths, the localization length decreases monotonically. Such a transition was indeed observed experimentally in a noninteracting bosonic gas (*30*). In contrast, truly random disorder will lead to single-particle localization in one dimension already for arbitrarily small disorder strengths. Previous numerical work indicates MBL in quasirandom systems to be similar to that obtained for a truly random potential (*36*).

Experiment

We experimentally realized the Aubry-André model by superimposing on the primary, short lattice ($\lambda_s = 532$ nm) a second, incommensurate disorder lattice with $\lambda_d = 738$ nm (thus, $\beta = \lambda_s/\lambda_d \approx 0.721$) and control J, Δ, and ϕ via lattice depths and relative phase between the two lattices (*37*). The interactions (U) between atoms in the two different spin states $|\uparrow\rangle$ and $|\downarrow\rangle$ are tuned via a magnetic Feshbach resonance (*37*). In total, this provides independent control of U, J, and Δ and enables us to continuously tune the system from an Anderson insulator in the noninteracting case to the MBL regime for interacting particles.

An additional long lattice ($\lambda_l = 1064$ nm $= 2\lambda_s$) forms a period-two superlattice (*39*, *40*) together with the short lattice and is used during the preparation of the initial CDW state and during detection (*37*). Deep lattices along the orthogonal directions [$\lambda_\perp = 738$ nm and $V_\perp = 36(1)E_R$] create an array of decoupled 1D tubes. Here, $E_R = h^2/(2m\lambda_{lat}^2)$ denotes the recoil energy, with h being Planck's constant, m the mass of the atoms, and λ_{lat} the respective wavelength of the lattice lasers.

We used a two-component degenerate Fermi gas of ^{40}K atoms, consisting of an equal mixture of 90×10^3 to 110×10^3 atoms in each of the two lowest hyperfine states $|F, m_F\rangle = |\frac{9}{2}, -\frac{9}{2}\rangle \equiv |\downarrow\rangle$ and $|\frac{9}{2}, -\frac{7}{2}\rangle \equiv |\uparrow\rangle$, at an initial temperature of $0.20(2)\,T_F$, where T_F is the Fermi temperature. The atoms were initially prepared in a finite temperature band insulating state (*41*), with up to 100 atoms per tube in the long and orthogonal lattices. We then split each lattice site by ramping up the short lattice in a tilted configuration (*37*) and subsequently ramped down the long lattice. This creates a CDW, in which there are no atoms on odd lattice sites but zero, one, or two atoms on each even site (*40*, *42*). This initial CDW is then allowed to evolve for a given time in the $8.0(2)E_R$ deep short lattice at a specific interaction strength U in the presence of disorder Δ. In a final step, we detected the number of atoms on even and odd lattice sites by using a band-mapping technique that maps them to different bands of the superlattice (*37*, *42*). This allows us to directly measure the imbalance $\mathcal{I}$, as defined in Eq. 1, in much larger systems than what is numerically feasible.

Results

We tracked the time evolution of the imbalance $\mathcal{I}$ for various interactions U and disorder strengths Δ (Fig. 2). At short times, the imbalance exhibits some dynamics consisting of a fast decay followed by a few damped oscillations. After a few tunneling times $\tau = h/(2\pi J)$, the imbalance approaches a stationary value. In a clean system ($\Delta/J = 0$), and for weak disorder, the stationary value of the imbalance approaches zero. For stronger disorder, however, this behavior changes dramatically, and the imbalance attains a nonvanishing stationary value that persists for all observation times. Because the imbalance must decay to zero on approaching thermal equilibrium at these high energies, the nonvanishing stationary value of $\mathcal{I}$ directly indicates nonergodic dynamics. Deep in the localized phase, in which unbiased numerical density-matrix renormalization group (DMRG) calculations are feasible because of the slow entanglement growth,

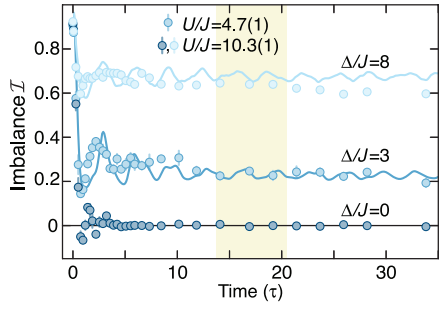

Fig. 2. Time evolution of an initial CDW. A CDW, consisting of fermionic atoms occupying only even sites, is allowed to evolve in a lattice with an additional quasirandom disorder potential. After variable times, the imbalance $\mathcal{I}$ between atoms on odd and even sites is measured. Experimental time traces (circles) and DMRG calculations for a single homogeneous tube (lines) (*37*) are shown for various disorder strengths Δ. Each experimental data point denotes the average of six different realizations of the disorder potential, and the error bars show the SD of the mean. The shaded region indicates the time window used to characterize the stationary imbalance in the rest of the analysis.

we found the stationary value obtained in the simulations to be in very good agreement with the experimental result. These simulations were performed for a single homogeneous tube without any trapping potentials (*37*). The stronger damping of oscillations observed in the experiment can be attributed to a dephasing caused by variations in J between different 1D tubes (*37*, *42*).

We experimentally observed an additional very slow decay of $\mathcal{I}$ on a time scale of several hundred tunneling times for all interaction strengths, which we attribute to the fact that our system is not perfectly closed owing to small background gas losses, technical heating, photon scattering, and coupling to neighboring

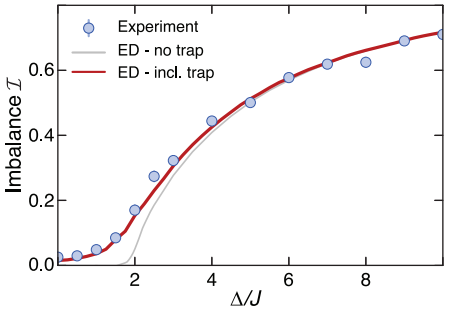

Fig. 3. Stationary values of the imbalance $\mathcal{I}$ as a function of disorder strength Δ for noninteracting atoms. The Aubry-André transition is at $\Delta/J = 2$. Circles show the experimental data, along with exact diagonalization (ED) calculations with (red line) and without (gray line) trap effects (*37*). Each experimental data point is the average of three different evolution times (13.7, 17.1, and 20.5 τ) and four different disorder phases ϕ, for a total of 12 individual measurements per point. To avoid any interaction effects, only a single spin component was used. The ED calculations are averaged over similar evolution times to the experiment and 12 different phase realizations. Error bars show the SD of the mean.

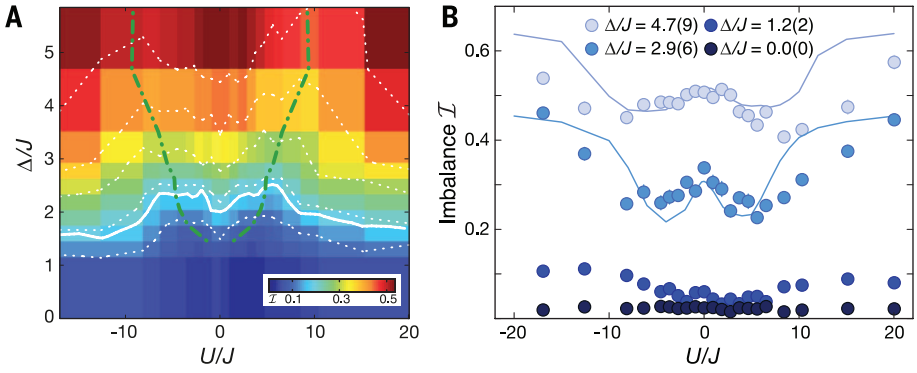

Fig. 4. Stationary imbalance for various interaction and disorder strengths. (**A**) Stationary imbalance $\mathcal{I}$ as a function of interactions U and disorder strength Δ. Moderate interactions reduce the degree of localization compared with the noninteracting or strongly interacting cases. The white dotted lines are contours of equal $\mathcal{I}$, and the solid white line is the contour of $\mathcal{I}$ matching the Aubry-André transition ($U = 0$ and $\Delta/J = 2$) extended to the interacting case. It indicates the MBL transition. The green dot-dashed line shows the fitted minima of $\mathcal{I}$ for each Δ (*37*). Each individual data point (vertices of the pseudo-color plot) is the average of the same 12 parameters as in Fig. 3. The color of each square represents the average imbalance of the four points on the corners. All data were taken with a doublon fraction of 34(2)%. (**B**) Cuts along four different disorder strengths. The effect of interactions on the localization gives rise to a characteristic "W" shape. Solid lines are the results of DMRG simulations for a single homogeneous tube. Error bars indicate the SD of the mean.

tubes (*37*, *43*). Another potential mechanism for delocalization at long times is related to the intrinsic SU(2) spin symmetry in our system (*44*). However, for the relevant observation times our numerical simulations do not indicate the presence of such a thermalization process.

To characterize the dependence of the localization transition on U and Δ, we focused on the stationary value of $\mathcal{I}$, plotted in Fig. 3 for noninteracting atoms and in Fig. 4 for interacting atoms. For noninteracting atoms (Fig. 3), the measured imbalance is compatible with extended states within the finite, trapped system for $\Delta/J \lesssim 2$. Above the critical point of the homogeneous Aubry-André model at $\Delta/J = 2$ (*38*), however, the measured imbalance strongly increases as the single-particle eigenstates become more and more localized. The observed transition agrees well with our theoretical modeling, including the harmonic trap (*37*).

The addition of moderate interactions slightly reduces the degree of localization compared with that of the noninteracting case; they decrease the imbalance $\mathcal{I}$ and hence increase the critical value of Δ necessary to cross the delocalization-localization transition (Fig. 4, A and B). We found that localization persists for all interaction strengths. For a given disorder, the imbalance $\mathcal{I}$ decreases up to a value of $U \sim 2\Delta$ before increasing again. For large $|U|$, the system even becomes more localized than in the noninteracting case. This can be understood qualitatively by considering an initial state consisting purely of empty sites and sites with two atoms (doublons): For sufficiently strong interactions, isolated doublons represent stable quasiparticles because the two atoms cannot separate and hence only tunnel with an effective second-order tunneling rate of $J_D = \frac{2J^2}{|U|} \ll J$ (*45*, *46*). This strongly increases the effective disorder $\propto \Delta/J_D \gg \Delta/J$ and promotes localization. In the experiment, the initial doublon fraction is well below one (*37*), and the density is finite, so that we observed a weaker effect. We found the localization dynamics and the resulting stationary values to be symmetric around $U = 0$, highlighting the dynamical $U \leftrightarrow -U$ symmetry of the Hubbard Hamiltonian for initially localized atoms (*47*). The effect of interactions can be seen in the contour lines (Fig. 4A, dotted white lines) as well as directly in the characteristic "W" shape of the imbalance at constant disorder (Fig. 4B), demonstrating the re-entrant behavior of the system (*22*). This behavior extends to our best estimate of the localization transition, which is shown in Fig. 4A as the solid white line.

We can gain additional insight into how localization changes with interaction strength by computing the growth of the entanglement entropy (*37*) between the two halves of the system during the dynamics (Fig. 5A). For long times, we observed a logarithmic growth of the entanglement entropy with time as $S(t) = S_{\text{offset}} + s_* \ln(t/\tau)$, which is characteristic of the MBL phase (*12*, *13*). The slope s_* is proportional to the bare localization length ξ_*, which in a weakly interacting system in the localized phase corresponds to the single-particle localization length. In general, ξ_* is the characteristic length over which the effective interactions between the conserved local densities decay (*17*, *18*) and connects to the many-body localization length ξ deep in the localized phase. In contrast to ξ, however, ξ_* is expected to remain finite at the transition (*48*). We found s_* to exhibit a broad maximum for intermediate interaction strengths (Fig. 5B), corresponding to a maximum in the thus inferred localization length. This maximum in turn leads to a minimum in the CDW value. Both the characteristic "W" shape in the imbalance and the maximum in the entanglement entropy slope are consequences of the maximum in localization length. Equivalent information on the localization properties as obtained from the entanglement entropy can be gained in experiments by monitoring the temporal decay of fluctuations around the stationary value of the CDW (*37*). Although we do not have sufficient sensitivity to measure these fluctuations in the current experiment, we expect them to be accessible to experiments with single-site resolution (*49*, *50*).

To systematically study the effect of the initial energy density on the MBL phase, we loaded the lattice using either attractive, vanishing, or repulsive interactions (Fig. 6), predominantly changing the number of doublons in the initial state (*37*). Because the initial state consists of fully localized particles only, the local energy density is directly given by the product of interaction strength U and doublon density. We found that for an interaction strength during the evolution of $|U/J| \leq 6$, the energy density does not substantially affect the localization properties, proving that MBL persists over a wide energy range. For $|U/J| > 8$, localization properties depend substantially on the doublon fraction because of the second emerging energy scale J_D, as discussed above. Thus, the localization transition can be tuned via changing the doublon fraction at large U. This constitutes a direct observation of a many-body mobility edge because the doublon density dominates the energy density.

For the case of repulsive loading, which results in a low fraction of doubly occupied sites, the imbalance for $U/J = 0$ and strong interactions match within error. Indeed, a rigorous mapping

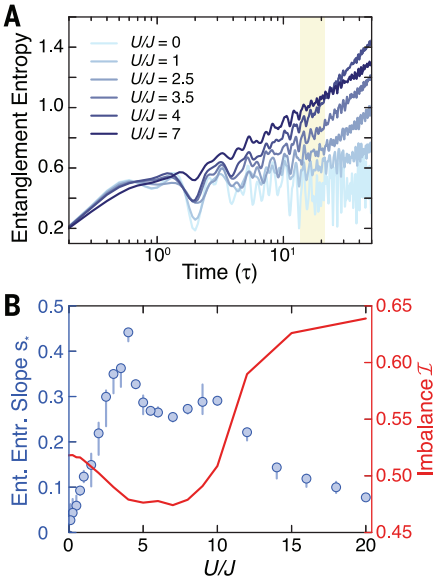

Fig. 5. Calculated growth of entanglement entropy and corresponding slope. (**A**) DMRG results of the entanglement entropy growth (*37*) for various interaction strengths and $\Delta/J = 5$. For long times, logarithmic growth characteristic of interacting MBL states is visible. The experimentally used evolution times indicated by the yellow shaded region are found to be in the region of logarithmic growth. (**B**) The slope of the logarithmic growth (circles), extracted by using linear fits up to the longest simulated time (50 τ) in (A), shows a nonmonotonic dependence on the interaction strength, which is correlated with the inverse of the steady-state value of the CDW order parameter (red line). Error bars reflect different initial starting times for the fit.

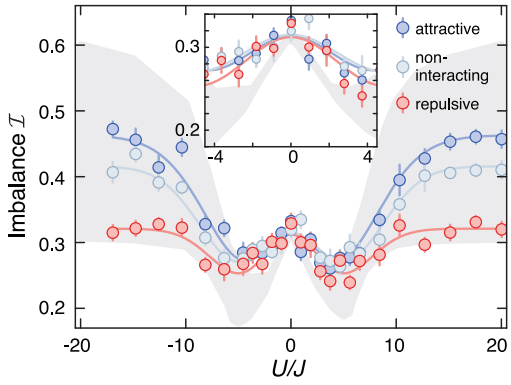

Fig. 6. Stationary imbalance $\mathcal{I}$ as a function of interaction strength during loading. Data were taken with disorder $\Delta/J = 3$. The loading interactions of $a_{load} = -89(2)\ a_0$ (attractive, where a_0 denotes Bohr's radius), $0(1)\ a_0$ (noninteracting), and $142(1)\ a_0$ (repulsive) correspond to initial doublon fractions of 51(1), 43(2), and 8(6)%, respectively (*39*). Each $\mathcal{I}$ value is the average of the same 12 parameters as in Fig. 3. Error bars show the SD of the mean. Solid lines are guides to the eye. The gray shaded area spans the limiting cases of 0 and 50% doublons, simulated by using DMRG for a single homogeneous tube.

can be made between the noninteracting system and the dynamics in the doublon-free subspace at strong interactions $|U/J| \to \infty$ (*37*). At very large interactions and high doublon fractions, the additional long time scales start to also compete with heating and loss processes, rendering the definition of stationary states challenging.

Conclusion

Our experimental demonstration of ergodicity breaking because of MBL paves the way for many further investigations. An interesting extension would be to use "true" random disorder created by, for example, an optical speckle pattern, as has been used to study Anderson localization (*27*). Another important next step is extending the present study to higher dimensions. Additional insight can also be gained by analyzing the full relaxation dynamics of local observables (*19*–*21*) in an experimental setup featuring single-site resolution (*49*, *50*). For instance, the decay of fluctuations of $\mathcal{I}$ with time could be directly measured, providing an even more direct connection to the entanglement entropy. Another important direction for future investigation is the effect of opening the system in a controlled way. This could be done, for example, by adding a near-resonant laser so as to deliberately enhance photon scattering or by using a Bose-Fermi mixture, in which excitations of the Bose-Einstein condensate form a well-controlled bath for the fermions. This will allow a systematic study of the critical dynamics associated with the MBL phase transition, in which the bath relaxation time now provides the only scale. Such a study would also allow the MBL phase to be clearly distinguished experimentally from classical glassy dynamics. The latter, unlike MBL, is insensitive to coupling of the system to an external bath.

REFERENCES AND NOTES

1. J. Lux, J. Müller, A. Mitra, A. Rosch, *Phys. Rev. A* **89**, 053608 (2014).
2. J. M. Deutsch, *Phys. Rev. A* **43**, 2046–2049 (1991).
3. M. Srednicki, *Phys. Rev. E Stat. Phys. Plasmas Fluids Relat. Interdiscip. Topics* **50**, 888–901 (1994).
4. M. Rigol, V. Dunjko, M. Olshanii, *Nature* **452**, 854–858 (2008).
5. B. Paredes *et al.*, *Nature* **429**, 277–281 (2004).
6. T. Kinoshita, T. Wenger, D. S. Weiss, *Nature* **440**, 900–903 (2006).
7. M. Gring *et al.*, *Science* **337**, 1318–1322 (2012).
8. P. W. Anderson, *Phys. Rev.* **109**, 1492–1505 (1958).
9. D. M. Basko, I. L. Aleiner, B. L. Altshuler, *Ann. Phys.* **321**, 1126–1205 (2006).
10. I. V. Gornyi, A. D. Mirlin, D. G. Polyakov, *Phys. Rev. Lett.* **95**, 206603 (2005).
11. J. Z. Imbrie, On many-body localization for quantum spin chains. http://arxiv.org/abs/1403.7837 (2014).
12. M. Žnidarič, T. Prosen, P. Prelovšek, *Phys. Rev. B* **77**, 064426 (2008).
13. J. H. Bardarson, F. Pollmann, J. E. Moore, *Phys. Rev. Lett.* **109**, 017202 (2012).
14. B. Bauer, C. Nayak, *J. Stat. Mech.* **09**, P09005 (2013).
15. R. Vosk, E. Altman, *Phys. Rev. Lett.* **110**, 067204 (2013).
16. M. Serbyn, Z. Papić, D. A. Abanin, *Phys. Rev. Lett.* **110**, 260601 (2013).
17. M. Serbyn, Z. Papić, D. A. Abanin, *Phys. Rev. Lett.* **111**, 127201 (2013).
18. D. A. Huse, R. Nandkishore, V. Oganesyan, *Phys. Rev. B* **90**, 174202 (2014).
19. F. Andraschko, T. Enss, J. Sirker, *Phys. Rev. Lett.* **113**, 217201 (2014).
20. R. Vasseur, S. A. Parameswaran, J. E. Moore, *Phys. Rev. B* **91**, 140202 (2015).
21. M. Serbyn, Z. Papić, D. A. Abanin, *Phys. Rev. B* **90**, 174302 (2014).
22. Y. Bar Lev, G. Cohen, D. R. Reichman, *Phys. Rev. Lett.* **114**, 100601 (2015).
23. A. Pal, D. A. Huse, *Phys. Rev. B* **82**, 174411 (2010).
24. D. S. Wiersma, P. Bartolini, A. Lagendijk, R. Righini, *Nature* **390**, 671–673 (1997).
25. Y. Lahini *et al.*, *Phys. Rev. Lett.* **100**, 013906 (2008).
26. T. Schwartz, G. Bartal, S. Fishman, M. Segev, *Nature* **446**, 52–55 (2007).
27. J. Billy *et al.*, *Nature* **453**, 891–894 (2008).
28. S. S. Kondov, W. R. McGehee, J. J. Zirbel, B. DeMarco, *Science* **334**, 66–68 (2011).
29. F. Jendrzejewski *et al.*, *Nat. Phys.* **8**, 398–403 (2012).
30. G. Roati *et al.*, *Nature* **453**, 895–898 (2008).
31. B. Deissler *et al.*, *Nat. Phys.* **6**, 354–358 (2010).
32. B. Gadway, D. Pertot, J. Reeves, M. Vogt, D. Schneble, *Phys. Rev. Lett.* **107**, 145306 (2011).
33. C. D'Errico *et al.*, *Phys. Rev. Lett.* **113**, 095301 (2014).
34. S. S. Kondov, W. R. McGehee, W. Xu, B. DeMarco, *Phys. Rev. Lett.* **114**, 083002 (2015).
35. M. Ovadia, D. Kalok, I. Tamir, S. Mitra, B. Sacepe, D. Shahar, Evidence for a finite temperature insulator. http://arxiv.org/abs/1406.7510 (2014).
36. S. Iyer, V. Oganesyan, G. Refael, D. A. Huse, *Phys. Rev. B* **87**, 134202 (2013).
37. Materials and methods are available as supplementary materials on *Science* Online.
38. S. Aubry, G. André, *Ann. Israel Phys. Soc.* **3**, 133 (1980).
39. J. Sebby-Strabley, M. Anderlini, P. S. Jessen, J. V. Porto, *Phys. Rev. A* **73**, 033605 (2006).
40. S. Fölling *et al.*, *Nature* **448**, 1029–1032 (2007).
41. U. Schneider *et al.*, *Science* **322**, 1520–1525 (2008).
42. S. Trotzky *et al.*, *Nat. Phys.* **8**, 325–330 (2012).
43. H. Pichler, A. J. Daley, P. Zoller, *Phys. Rev. A* **82**, 063605 (2010).
44. R. Vasseur, A. C. Potter, S. A. Parameswaran, *Phys. Rev. Lett.* **114**, 217201 (2015).
45. K. Winkler *et al.*, *Nature* **441**, 853–856 (2006).
46. S. Trotzky *et al.*, *Science* **319**, 295–299 (2008).
47. U. Schneider *et al.*, *Nat. Phys.* **8**, 213–218 (2012).
48. R. Vosk, D. A. Huse, E. Altman, Theory of the many-body localization transition in one dimensional systems. http://arxiv.org/abs/1412.3117 (2014).
49. W. S. Bakr, J. I. Gillen, A. Peng, S. Fölling, M. Greiner, *Nature* **462**, 74–77 (2009).
50. J. F. Sherson *et al.*, *Nature* **467**, 68–72 (2010).
51. F. Essler, H. Frahm, F. Göhmann, A. Klümper, V. Korepin, *The One-Dimensional Hubbard Model* (Cambridge Univ. Press, Cambridge, UK, 2005).
52. C. Gramsch, M. Rigol, *Phys. Rev. A* **86**, 053615 (2012).

ACKNOWLEDGMENTS

We acknowledge useful discussions with F. Essler and technical assistance by D. Garbe and F. Görg during the setup of the experiment. We acknowledge financial support by the Deutsche Forschungsgemeinschaft (FOR801, Deutsch-Israelisches Kooperationsprojekt Quantum phases of ultracold atoms in optical lattices), the European Commission (UQUAM and AQuS), the U.S. Defense Advanced Research Projects Agency (Quantum Emulations of New Materials Using Ultracold Atoms), the Minerva Foundation, ISF grant no. 1594/11, Nanosystems Initiative Munich (NIM), and the Swiss Society of Friends of the Weizmann Institute.

SUPPLEMENTARY MATERIALS

www.sciencemag.org/content/349/6250/842/suppl/DC1
Supplementary Text
Figs. S1 to S9
References (*53*–*62*)

22 January 2015; accepted 21 July 2015
Published online 30 July 2015
10.1126/science.aaa7432

Observation of many-body localization of interacting fermions in a quasirandom optical lattice

Michael Schreiber, Sean S. Hodgman, Pranjal Bordia, Henrik P. Lüschen, Mark H. Fischer, Ronen Vosk, Ehud Altman, Ulrich Schneider and Immanuel Bloch

Science **349** (6250), 842-845.
DOI: 10.1126/science.aaa7432originally published online July 30, 2015

Making interacting atoms localize

Disorder can stop the transport of noninteracting particles in its tracks. This phenomenon, known as Anderson localization, occurs in disordered solids, as well as photonic and cold atom settings. Interactions tend to make localization less likely, but disorder, interactions, and localization may coexist in the so-called many-body localized state. Schreiber *et al.* detect many-body localization in a one-dimensional optical lattice initially filled with atoms occupying alternating sites. Externally induced disorder and interactions prevented the system from evolving quickly to a state with a single atom on each site.

Science, this issue p. 842